JAERI - M
88-006

LOWER HYBRID CURRENT DRIVE FOR INTOR HIGH DENSITY AND HIGH TEMPERATURE OPERATION

— RESULTS OF THE BENCHMARK CALCULATION FOR INTOR —

February 1988

Akiyoshi HATAYAMA*, Kenkichi USHIGUSA, Tsuyoshi IMAI and Masayoshi SUGIHARA

日 本 原 子 力 研 究 所
Japan Atomic Energy Research Institute

JAERI-Mレポートは，日本原子力研究所が不定期に公刊している研究報告書です。
入手の問合わせは，日本原子力研究所技術情報部情報資料課（〒319-11茨城県那珂郡東海村）あて，お申しこしください。なお，このほかに財団法人原子力弘済会資料センター（〒319-11 茨城県那珂郡東海村日本原子力研究所内）で複写による実費頒布をおこなっております。

JAERI-M reports are issued irregularly.
Inquiries about availability of the reports should be addressed to Information Division, Department of Technical Information, Japan Atomic Energy Research Institute, Tokai-mura, Naka-gun, Ibaraki-ken 319-11, Japan.

編集兼発行　日本原子力研究所
印　　刷　㈱原子力資料サービス

JAERI-M 88-006

Lower Hybrid Current Drive for INTOR High Density and High Temperature Operation - Results of the Benchmark Calculation for INTOR -

Akiyoshi HATAYAMA,* Kenkichi USHIGUSA, Tsuyoshi IMAI and Masayoshi SUGIHARA

Department of Large Tokamak Research
Naka Fusion Research Establishment
Japan Atomic Energy Research Institute
Naka-machi, Naka-gun, Ibaraki-ken

(Received January 7, 1988)

Lower hybrid current drive for INTOR high density and high temperature plasma has been studied. The calculational model based on a toroidal ray tracing code and 1-D Fokker-Planck code. RF current profiles are generally not centrally peaked, but localized near plasma surface ($r/a \sim 0.65 - 1.0$) for the parameter range ($\bar{n}_e \sim 5 - 7.5 \times 10^{19}$ m^{-3} and $\bar{T}_e \sim 10 - 20$ keV) calculated. Effects of wave spectra on the current profile and the current drive efficiency have been studied systematically using the Gaussian spectra with different centeral values $N_{/\!/0}$ and the widths $\Delta N_{/\!/0}$. The effect of wave launched angle has been also studied. Wave penetration is shown to be effectively improved for the top launched case for $\bar{n}_e = 5 \times 10^{19}$ m^{-3} and $\bar{T}_e = 12.5$ keV.

Keywords: INTOR, Lower Hybrid Wave, Current Drive, Current Profile, Wave Spectrum

---

* Toshiba Corporation

JAERI－M 88－006

ＩＮＴＯＲ高温・高密度運転時のＬＨＲＦ電流駆動
－ ＩＮＴＯＲに対するベンチマーク計算結果 －

日本原子力研究所那珂研究所臨界プラズマ研究部
畑山明聖*・牛草健吉・今井　剛・杉原正芳

（1988 年 1 月 7 日受理）

ＩＮＴＯＲの高温・高密度プラズマに対する低域混成波電流駆動の可能性について検討した。電子密度 $\bar{n}_e \sim 5 - 7.5 \times 10^{19}\ m^{-3}$，電子温度 $\bar{T}_e \sim 10 - 20\ keV$ の範囲で波動の伝搬軌道解析コード及び１次元フォッカープランクコードを用いて解析した結果，一般に得られるＲＦ駆動電流分布は，プラズマ表面近傍の領域に局在化した分布となる。合せて入射ＲＦパワー・スペクトラムの形状が駆動電流分布及び電流駆動効率に及ぼす影響をガウス分布のスペクトラムを用いて系統的に調べた。また，ＲＦの入射角が駆動電流分布に及ぼす効果を調べた結果，トーラス上方から入射した場合には電流分布がかなり改善されることが示された。

那珂研究所：〒 311－02　茨城県那珂郡那珂町大字向山 801－1
＊（株）東芝

Contents

目　　次

1. Introduction

Non-inductive current drive would be one indispensible technology to make the tokamak system a more attractive reactor candidate. Non-inductive current drive using lower hybrid waves has been intensively studied in many tokamak experiments. These experiments have demonstrated that plasma current can be maintained by lower hybrid waves alone with high current drive efficiency in most cases. It has been also demonstrated that the plasma current can be ramped up or the OH-transformer can be recharging by applying larger amounts of RF power than necessary for maintaining a steady state current. Lower hybrid assisted ramp-up can be reduce the volt-second requirements, whereas OH recharging enables quasi-steady state operation of a tokamak reactor. In addition to these small- and medium-sized tokamak experiments, recent JT-60 lower hybrid current drive experiments [1,2] have demonstrated that lower hybrid current drive is a promissing candidate for non-inductive current drive for the reactor relevant large tokamaks.

In the present report, we investigate the potentiality of lower hybrid current drive for INTOR high density and high temperature operation. Benchmark problem, which is offered in INTOR workshop [3], for high density and high temperature case has been solved by computer simulation code. The code is based on a ray tracing code and a 1-D Fokker-Planck code. Effects of wave spectra on the wave penetration and the RF driven current profile have been studied systematically using Gaussian profile with different central values of refractive index $N_{//0}$ and the width $\Delta N_{//}$. The effects of wave launched angle on the RF current profile have been also studied.

In sec. 2, a brief discription of the numerical code used to calculate the benchmark problem is given. In sec. 3, main plasma parameters of INTOR benchmark problem and RF parameters used in the calculation are described. Numerical results and summary of the present study are given in Sec. 4 and Sec. 5, respectively.

2. Brief description of the numerical code

The employed model consists of a toroidal ray tracing code and a 1-D Fokker-Planck code. Toroidal ray trajectories are calculated using the dispersion relation which includes electromagnetic and warm plasma effects. The input power spectrum for the ray tracing calculations is specified in two ways;

1) Gaussian distribution,

$$P\ (N_{//}) = P_0 \exp\ [\ -\ \frac{(N_{//} - N_{//_0})^2}{(\Delta N_{//}/2)^2}\ ], \qquad (2.1)$$

where $N_{//0}$ is the center value of the parallel refractive index $N_{//}$, $\Delta N_{//}$ the width of the spectrum. The normalization constant P_0 is determined by the condition $\int P(N_{//})\ dN_{//} = P_{rf}$, where P_{rf} is the total input of the RF power.

2) Brambilla spectrum - the spectrum calculated by the Brambilla theory [4].

The specified spectrum is divided into typically 100 - 200 intervals $\Delta N_{//_j}$ (j=1, 2, ... , 200). A single ray is launched for each $N_{//_j}$ intervals, wieghted to the appropriate power which is included in the interval $\Delta N_{//_j}$. Each ray is followed separately as it propagates into the plasma. The power absorption by electrons and the resultant RF current are calculated by 1-D quasilinear Fokker - Planck equation in the steady state, using the results of the ray tracing calculations.

3. Numerical Parameters for INTOR Benchmark Calculations

Typical plasma and device parameters used in the present study for INTOR are summarized as follows;

Major radius: $R_0 = 4.9$ m,

Aspect ratio: $A = 4.2$,

Toroidal magnetic field: $B_0 = 5.5$ T,

Total plasma current: $I_p = 8$ MA

Fuel gas: D_2

Effective charge $Z_{eff} = 1.5$

Profiles of the electron density $n_e(r)$, the electron temperature $T_e(r)$, the radial, the poloidal and the toroidal magnetic field $B_r(r)$, $B_\theta(r)$ and $B_\phi(r)$ are assumed to be given by,

$$n_e(r) = n_{e0}[1-(r/a)^2] + n_{eb},\ n_{eb} = 0.05\ n_{e0}, \tag{3.1}$$

$$T_e(r) = T_{e0}[1-(r/a)^2] + T_{eb},\ T_{eb} = 0.05\ T_{e0}, \tag{3.2}$$

$$B_r(r) = 0, \tag{3.3a}$$

$$B_\theta(r) = \frac{\mu_0 I_p}{\pi r}\left(1 - \frac{r^2}{2a^2}\right)\frac{r^2}{a^2}, \tag{3.3b}$$

$$B_\phi(r) = \frac{B_0}{1 + (r/R_0)\cos\theta}\ . \tag{3.3c}$$

The plasma cross section is divided into 30 equally spaced radial zones and the electron velocity distribution function f, the RF current density j_{rf} and the absorption power P_{abs} of electron are calculated at each of these radial locations.

RF frequency is chosen as f = 4 GHz based on the present data bases for the density limit of LHCD [5] and the total RF power $P_{rf} = 15$ MW is assumed to be injected in the present calculations.

4. Numerical Results

First we study the effects of wave spectra on the RF current profile and the current drive efficiency for INTOR high temperature and high density case. The wave spectra radiated from the launcher is assumed to be Gaussian distribution and is given by eq. (2.1). Average electron temperature and density are assumed to be $\bar{T}_e$ = 12.5 keV and $\bar{n}_e$ = 0.75 x $10^{20}m^{-3}$, respectively.

Figure 1 shows the radial profiles of the RF current for different wave spectra. The center value $N_{//0}$ of the wave spectrum is changed from $N_{//0}$ = 1.5 to 2.5, while the width of the spectra $\Delta N_{//0}$ is fixed to be $\Delta N_{//0}$ = 0.5 in all cases. Calcualted current profiles are not centrally peaked, but localized near plasma surface around r = 0.8 - 1.17 m for all cases, as shown in Fig. 1. This is partly because the strong localization of power absorption and partly because the limitation of the wave accessibility.

For large $N_{//0}$ case, the localization of the current profile is mainly due to the strong localization of power absorption. For small $N_{//0}$ case, the wave penetration is slightly improved, but the RF current profile is still localized near plasma surface. By decreasing $N_{//0}$, the absorption region goes into more interior. However, the limitation of the wave accessibility becomes more severe. Thus, before reaching such a strong absorption region, the wave is reflected. As a result, RF current profile is still localized near plasma peripheral region and the driven current becomes smaller compared with the case for larger $N_{//0}$ as shown in Fig. 1.

Figure 2 shows the $N_{//0}$ dependences of the current drive efficiency η_{cd} and the single path absorption rate η_{abs}, where η_{cd} and η_{abs} are defined as $\eta_{cd} = I_{rf}/P_{abs}$ and $\eta_{abs} = P_{abs}/P_{rf}$ and I_{rf}, P_{abs}, P_{rf} are the total RF current, the absorption power to electrons, and the total RF input power, respectively.

The input RF power is completely absorbed for the cases $N_{//0} \gtrsim 2$ and the single path power absorption rate becomes $\eta_{abs} = 1$. However, for the small $N_{//0}$ cases ($N_{//0} \lesssim 2$), η_{abs} decreases with $N_{//0}$ due to the increase of the inaccessible part of the wave spectrum as mentioned above. The current drive efficiency η_{cd} increases with $N_{//0}$. This is mainly due to the local density effect, i.e., with increasing $N_{//0}$, the input RF power is absorbed more outer region, where the density is smaller, and hence the efficiency increases. In order to make this effect more clear, here we define a local average density $\bar{n}_e^{loc}$ which is given by

$$\bar{n}_e^{loc} = \int_{r_m}^{r_M} n_e(r)dVp \Big/ \int_{r_m}^{r_M} dVp \tag{4.1}$$

where $n_e(r)$ is given by eq. (3.1) and r_m and r_M are the minimum and the maximum radial position for the localized profile of the RF current shown in Fig. 1. The current drive efficiency multiplied by $\bar{n}_e^{loc}$, $\eta_{local} \equiv \bar{n}_e^{loc} \times \eta_{cd}$, is shown in Fig. 3. η_{local} decreases with $N_{//0}$.

We have also calculated the efficiency for the case of almost uniform density profile. In this case, the density and temperature profiles are assumed to be given as follows;

$$n_e(r) = n_{e0}(1-r^2/a^2)^{0.1} + 0.05n_{e0}, \tag{4.2}$$

$$T_e(r) = T_{e0}(1-r^2/a^2)^{0.1} + 0.05T_{e0}, \tag{4.3}$$

The results for the current drive efficiency are shown in Fig. 3 for the case $\bar{n}_e = 5.0 \times 10^{18} m^{-3}$ and $\bar{T}_e = 10$ keV. Comparison is also given with the results obtained from the simple analytic expression by Fisch and Karney [6.7].

$$\eta_{cd} = I_{rf}/P_{abs} = \mu/\bar{n}_e(10^{20}\ m^{-3})R(m)\langle N_{//}^2\rangle, \tag{4,4}$$

where $1/\langle N_{//}^2\rangle = 0.5[(N_{//1}/N_{//2})^2-1]/N_{//1}^2 \ln(N_{//1}/N_{//2})$ and $\mu = 31.2/(Z_{eff}+2) \times \ln\Lambda$.

To obtain this expression, uniform current density and power absorption profiles and a wave spectrum of rectangular shape with the upper and lower bounds $N_{//1}$ and $N_{//2}$ have been assumed. The correction factor from the 2-D Fokker-Planck calculation has not been taken into account in eq. (4.4). To calculate the value of eq. (4.4), we put $N_{//1,2} = N_{//0} \pm \Delta N_{//}/2$. With these assumptions, the calculational results and theoretical results agree within a factor of 2 as shown in Fig. 4. The difference is considered to be mainly due to the difference of the shape of assumed wave spectrum. Especially, for small $N_{//0}$ - spectrum, launched spectrum is significantly changed in the plasma due to the constraint of the accessibility condition mentioned above.

Figure 5 shows the dependence of η_{cd} and η_{abs} on the spectrum width $N_{//0}$. In these cases, $N_{//0}$ is fixed and $N_{//0} = 1.75$, while $\Delta N_{//0}$ is changed from 0.5 to 2.5. The efficiency increases with $\Delta N_{//}$. By increasing $\Delta N_{//}$, large $N_{//}$ part of the spectrum increases. The power absorption begins more external low temperature region, as shown in Fig. 6. In such a low temperature region, the density is also smaller, and then the efficiency increases.

Dependences of the current drive efficiency and the RF current profile on the average electron temperature have been also studied using the fixed temperature profile given by eq. (3.2). Gaussian spectrum with $N_{//0} = 2.0$ and $N_{//0} = 0.5$ has been used in all cases. The average electron density is assumed to be $\bar{n}_e = 0.75 \times 10^{20} m^{-3}$. The results for the current drive efficiency η_{cd} and RF current profile are shown in Fig. 7 and Fig. 8, respectively. The higher the temperature is, the more external are the absorption and the resultant RF current profile, where the density is smaller. Hence the efficiency becomes larger.

Figure 9 shows the $\bar{n}_e$ dependences of η_{cd} and η_{abs} for $\bar{T}_e = 10$ keV and

$\bar{T}_e$ = 20 keV. The density and temperature profiles are fixed and given by eqs.(3.1) and (3.2). Gaussian spectrum with $N_{//0}$ = 1.75 and $\Delta N_{//0}$ = 0.5 has been used in the calculation. η_{abs} decreases with increasing the density because of the increase of the inaccessible part of the spectrum, especially, for the low temperature case. In this case the strong absorption region is further interior to the point where the main part of the spectrum can not be accessible, as seen from the comparison of the results for the RF current profiles shown in Fig. 10.

Finally, the effects of the launched angle θ_{inj} in the poloidal direction on the RF current profile have been studied. Figure 11 shows the radial profile of the RF current for $\theta_{inj} = 0^{\circ}$ (usual horizontal launch). In Fig. 11, (a) and (b) correspond to the cases for $N_{//0}$ = 2.0 and $N_{//0}$ = 1.8, respectively. In the present calculation, the launched spectra have been given by more realistic way, i.e., the spectra are specified by the Brambilla theory [1]. The total RF power P_{rf} = 15 MW is injected via 8 waveguide arrays with 4 horizontal rows. The peak value of the spectrum $N_{//0}$ is varied by changing the width of the waveguide, according to the relation, $N_{//0} = [c/f \cdot (b_p+d_p)] \cdot \Delta\phi/2\pi$, where c is the velocity of light and b_p+d_p is the width of the waveguide. The relative width $\Delta N_{//}/N_{//0}$ is almost unchanged and $\Delta N_{//}/N_{//0} \sim 1$ for all cases.

The RF current profiles for (a) and (b) in Fig. 11 are not centrally praked, but localized near plasma boundary as in the case of Gaussian spectra shown above. In Fig. 11, broken line shows the current density $j_{rf}^{-}(r)$ which is opposite direction to $j_{rf}^{+}(r)$ driven by the main robe ($N_{//}$ >1) of the spectrum. This is due to the existence of the negative part of the spectrum ($N_{//}^{-}$ <-1) of the launched spectrum. Since the absolute value $|N_{//}^{-}|$ for the negative part of the spectrum is larger than $N_{//0}$ and electron temperature is relatively low in the plasma edge region, $j_{rf}^{-}(r)$ is

localized further outer region compared with $j^{+}_{rf}(r)$ as shown in Fig. 11.

Inaddition to the case of the horizontal wave injection ($\theta_{inj} = 0^{o}$) shown above, the calculations are carried out for the case of vertical wave injection with the injection angle $\theta_{inj} = 90^{o}$(top launch). The results are shown in Fig. 12. Figures 12(a) and (b) correspond to the cases of (a) $N_{//0} = 2.0$ and (b) $N_{//0} = 1.8$, respectively, in the same way as in Fig. 11. The wave penetration is improved effectively by changing the injection angle from $\theta_{inj} = 0^{o}$ (horizontal launch) to $\theta_{inj} = 90^{o}$ (top launch), especially in the case (b).

The improvement of the wave penetration is explained as follow. The change in parallel refractive indiex $N_{//}$ along the way trajectory is shown in Fig. 13 for the case (a) horizontal launch ($\theta_{inj} = 0^{o}$) and (b) top launch ($\theta_{inj} = 90^{o}$), respectively. For the top launched case, $N_{//}$ initially decreases, while $N_{//}$ increases for the horizontal launched case. Thus the parallel phase velocity of the injected waves increases for the case $\theta_{inj} = 90^{o}$ in outer region, where plasma electron temperature is relatively low. These high phase velocity waves are not able to interact with the plasma electron in such a low temperature region. Thus the wave energy is not damped and penetrate futher interior in the plasma.

5. Summary

Potentiality of lower hybrid current drive for INTOR steady state operation in high density and high temperature ($\bar{n}_e \sim 0.75\times10^{20}$ m^{-3}, $\bar{T}_e \sim$ 10-20 keV) plasmas has been studied. The calculational model consists of three coupled numerical codes;

1) code based on the Brambilla theory for wave spectra and coupling

2) toroidal ray tracing code for wave propagation

3) 1-D Fokker-Planck code for power absorption

The model estimates the absorption power and RF currents along the single ray path for given density and temperature profiles. Wave frequency was chosen as f = 4 GHz based on the present data bases for the density limit for LHCD.

Calculated current profiles were generally not centrally peaked, but localized near plasma surface (r~0.8-1.1 m).

Effects of wave spectra for the current profile and current drive efficiency have been studied systematically by assuming the wave spectra to be Gaussian profile with the different central value $N_{//0}$ and the spectrum width $\Delta N_{//}$.

For large $N_{//0}$ ($\sim$2.0-2.5) case, the localization of the current profile is mainly due to the strong localization of power absorption. By decreasing $N_{//0}$, the absorption region goes into more interior. However, the limitation of the wave accessibility becomes more severe. Thus, before reaching such a strong absorption region, the wave is reflected. As a result, RF current profile is slightly improved, but is still localized near plasma peripheral region and the driven current becomes smaller compared with the case for larger $N_{//0}$.

We also investigated the effect of the wave launched angle for $\bar{n}_e$ = 0.5×10^{20} m^{-3} and $\bar{T}_e$ = 12.5 keV. Wave penetration was shown to be effectively improved for θ_{inj} = 90° (top launch) with compared to the case θ_{inj} = 0° (horizontal launch).

Acknowledgements

The authors wish to express thanks to Drs. S. Mori, K. Tomabechi, M. Yoshikawa and S. Tamura for their continuous encouragements.

References

1) T. Imai and JT-60 team: Proc. of 11th Int. Conf. on Plasma Physics and Controlled Nuclear Fusion Research, IAEA-CN-47/K-I-2, Kyoto, Japan, Nov. 1986.

2) Y. Yoshino and JT-60 team: Proc. of the 14th European Conf. on Controlled Fusion and Plasma Physics, Madrid, Spain, June 1987.

3) INTOR Group: International Tokamak Reactor, Phase IIA Part 3, Session XIV Report, Dec. 1986.

4) M. Brambilla: Nucl. Fusion 16(1976)47.

5) L.H. Sverdrup and P.M. Bellan: Phys. Rev. Lett. 59(1987)1197.

6) N.J. Fisch: Phys. Rev. Lett. 41(1978)873.

7) N.J. Fisch and C.F.F. Karney: Phys. Fluids 24(1981)27.

We also investigated the effect of the wave launched angle for $\bar{n}_e$ = 0.5×10^{20} m^{-3} and $\bar{T}_e$ = 12.5 keV. Wave penetration was shown to be effectively improved for $\theta_{inj} = 90^{\circ}$ (top launch) with compared to the case $\theta_{inj} = 0^{\circ}$ (horizontal launch).

Acknowledgements

The authors wish to express thanks to Drs. S. Mori, K. Tomabechi, M. Yoshikawa and S. Tamura for their continuous encouragements.

References

1) T. Imai and JT-60 team: Proc. of 11th Int. Conf. on Plasma Physics and Controlled Nuclear Fusion Research, IAEA-CN-47/K-I-2, Kyoto, Japan, Nov. 1986.

2) Y. Yoshino and JT-60 team: Proc. of the 14th European Conf. on Controlled Fusion and Plasma Physics, Madrid, Spain, June 1987.

3) INTOR Group: International Tokamak Reactor, Phase IIA Part 3, Session XIV Report, Dec. 1986.

4) M. Brambilla: Nucl. Fusion 16(1976)47.

5) L.H. Sverdrup and P.M. Bellan: Phys. Rev. Lett. 59(1987)1197.

6) N.J. Fisch: Phys. Rev. Lett. 41(1978)873.

7) N.J. Fisch and C.F.F. Karney: Phys. Fluids 24(1981)27.

We also investigated the effect of the wave launched angle for $\bar{n}_e$ = 0.5×10^{20} m^{-3} and $\bar{T}_e$ = 12.5 keV. Wave penetration was shown to be effectively improved for $\theta_{inj} = 90^{\circ}$ (top launch) with compared to the case $\theta_{inj} = 0^{\circ}$ (horizontal launch).

Acknowledgements

The authors wish to express thanks to Drs. S. Mori, K. Tomabechi, M. Yoshikawa and S. Tamura for their continuous encouragements.

References

1) T. Imai and JT-60 team: Proc. of 11th Int. Conf. on Plasma Physics and Controlled Nuclear Fusion Research, IAEA-CN-47/K-I-2, Kyoto, Japan, Nov. 1986.

2) Y. Yoshino and JT-60 team: Proc. of the 14th European Conf. on Controlled Fusion and Plasma Physics, Madrid, Spain, June 1987.

3) INTOR Group: International Tokamak Reactor, Phase IIA Part 3, Session XIV Report, Dec. 1986.

4) M. Brambilla: Nucl. Fusion 16(1976)47.

5) L.H. Sverdrup and P.M. Bellan: Phys. Rev. Lett. 59(1987)1197.

6) N.J. Fisch: Phys. Rev. Lett. 41(1978)873.

7) N.J. Fisch and C.F.F. Karney: Phys. Fluids 24(1981)27.

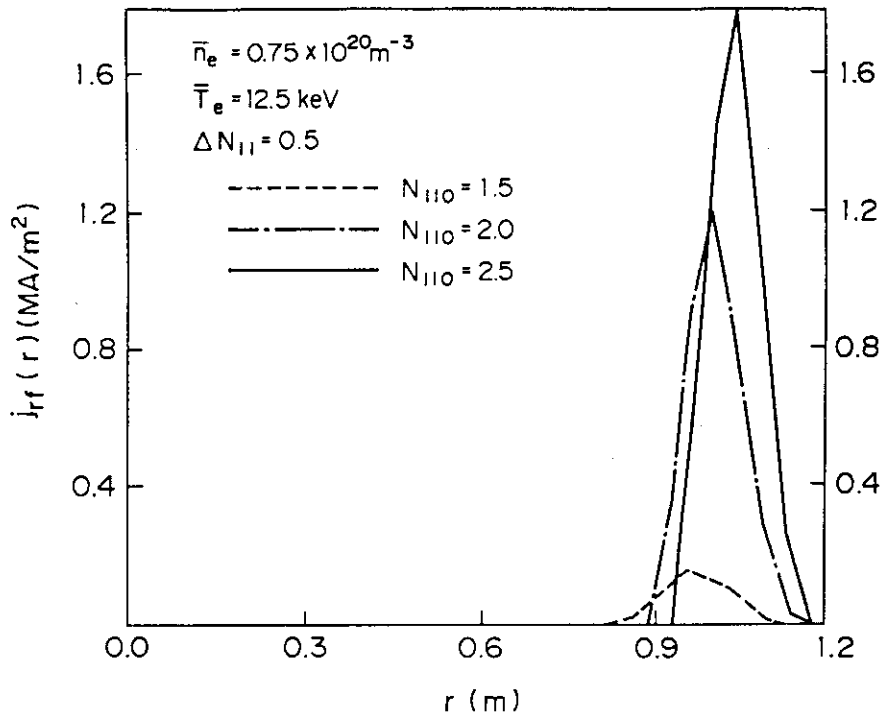

Fig. 1 Radial profile of the RF driven current for the different central values $N_{//0}$ of the wave spectrum.

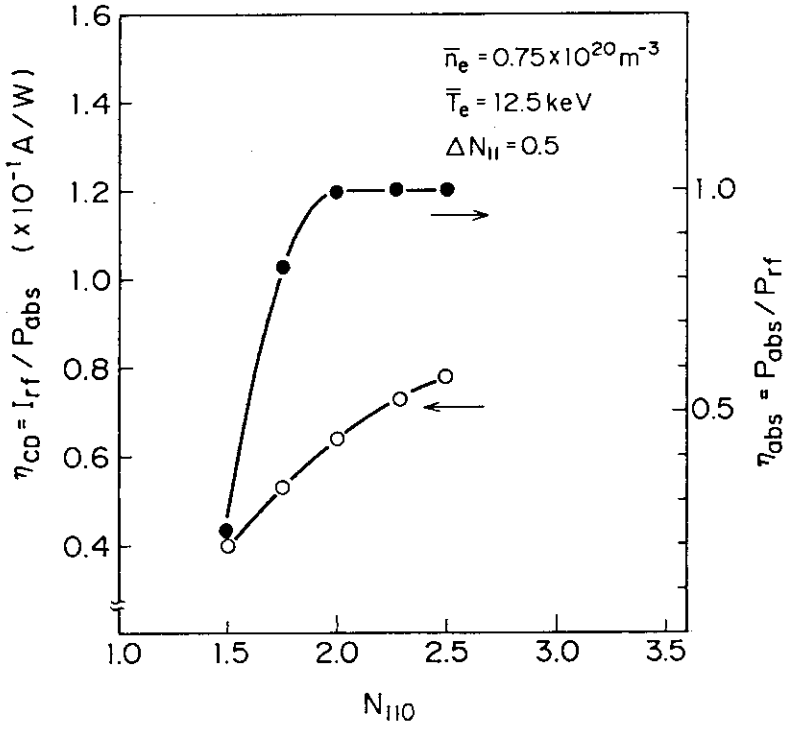

Fig. 2 Dependences of the current drive efficiency η_{cd} and the single path absorption rate η_{abs} on $N_{//0}$.

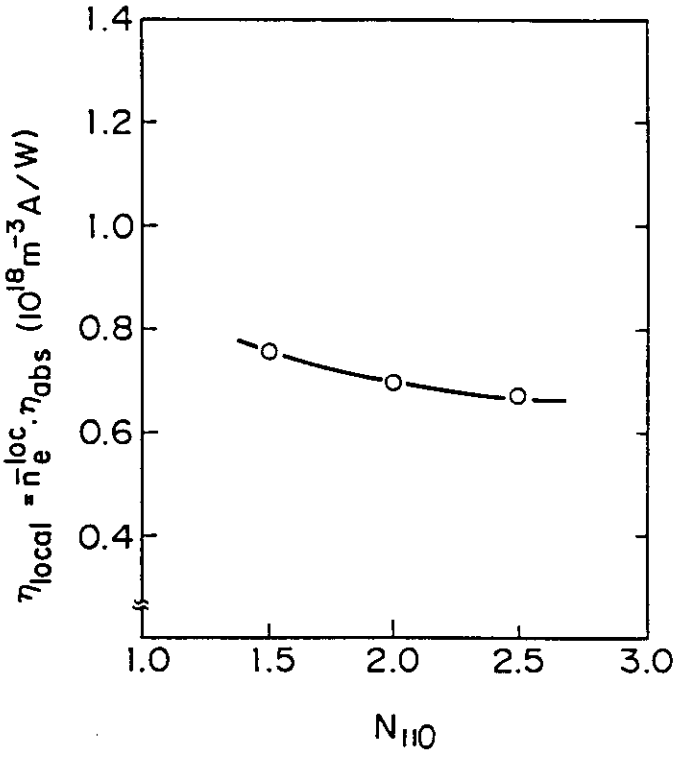

Fig. 3 Dependence of the current drive efficiency η_{local} on $N_{//0}$. η_{local} is defined by $\eta_{local} = \bar{n}_e^{-loc} \times \eta_{cd}$, where $\bar{n}_e^{-loc}$ is the density averaged over the localized region of the RF current.

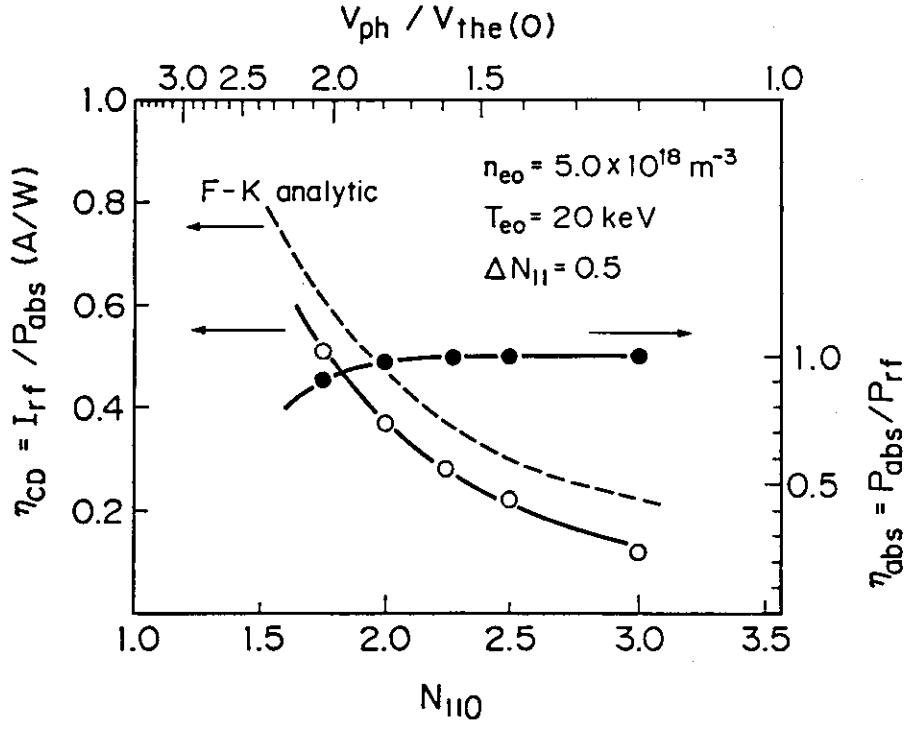

Fig. 4 Dependence of η_{cd} and η_{abs} on the $N_{//0}$ for the uniform density and temperature profiles [eqs. (4.2) and (4.3)]. The result obtained from the simple analytic expression by Fisch and Karney is also shown in the figure.

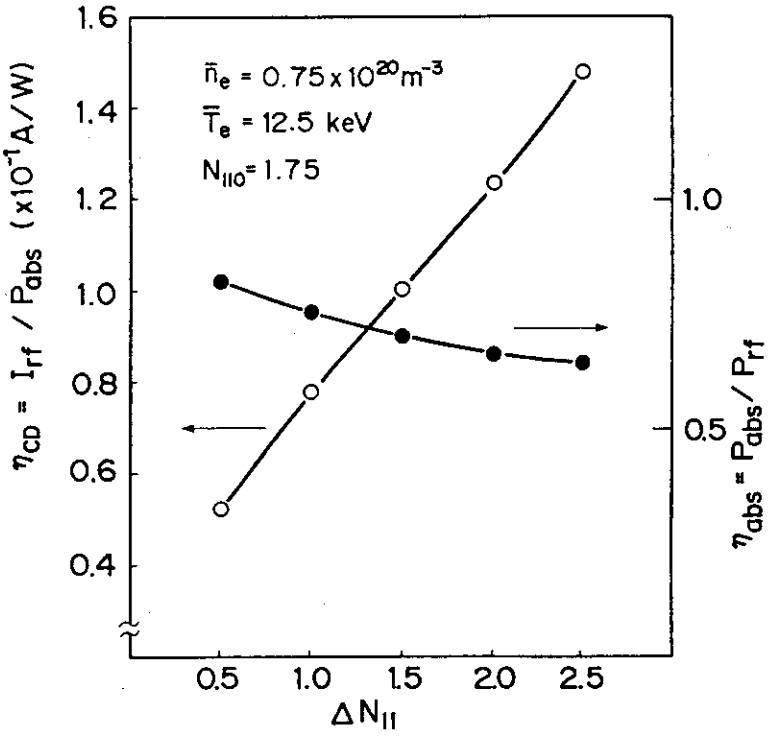

Fig. 5 Dependence of η_{cd} and η_{abs} on the spectrum width $\Delta N_{/\!/}$.

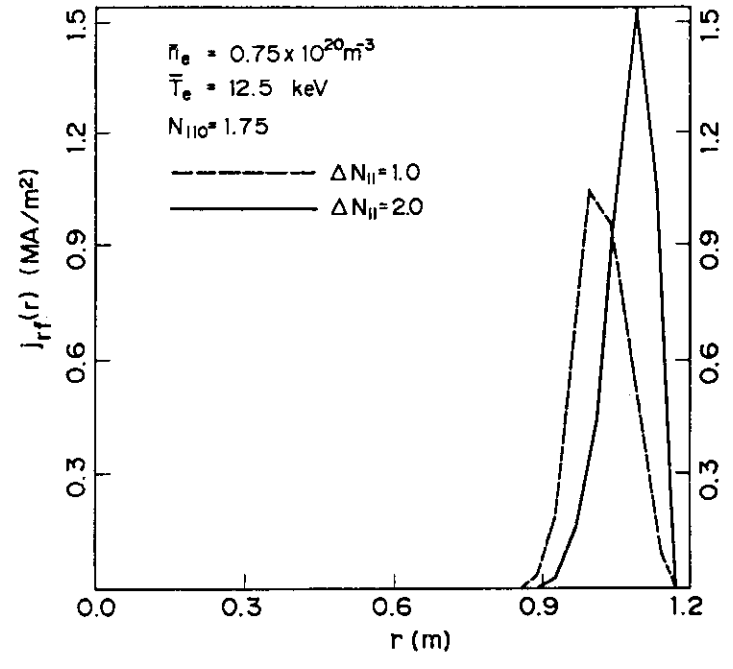

Fig. 6 Radial profile of the RF current for the different values of $\Delta N_{/\!/}$.

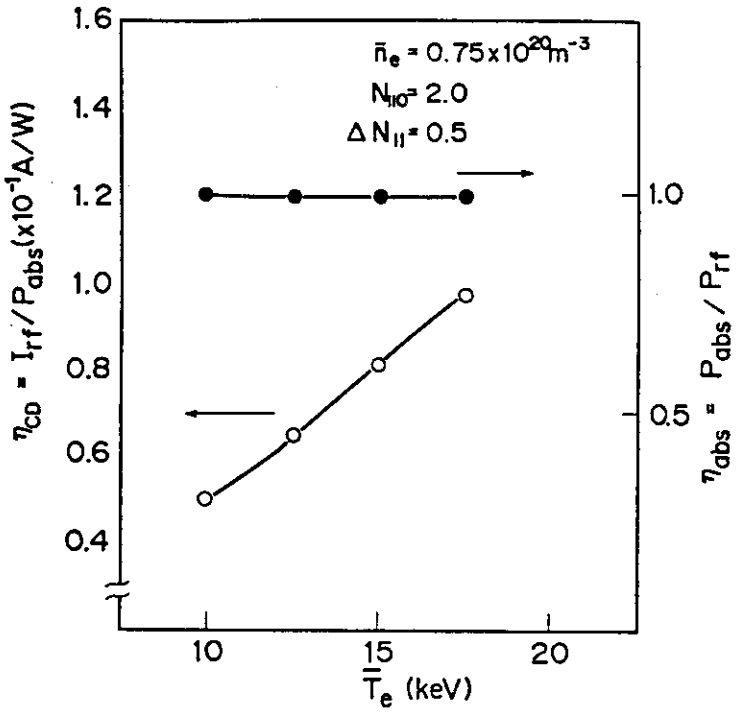

Fig. 7 Dependence of η_{cd} and η_{abs} on the average electron temperature $\bar{T}_e$. Gaussian power spectrum with $N_{\parallel 0}$ = 2.0 and $\Delta N_{\parallel 0}$ = 0.5 has been used.

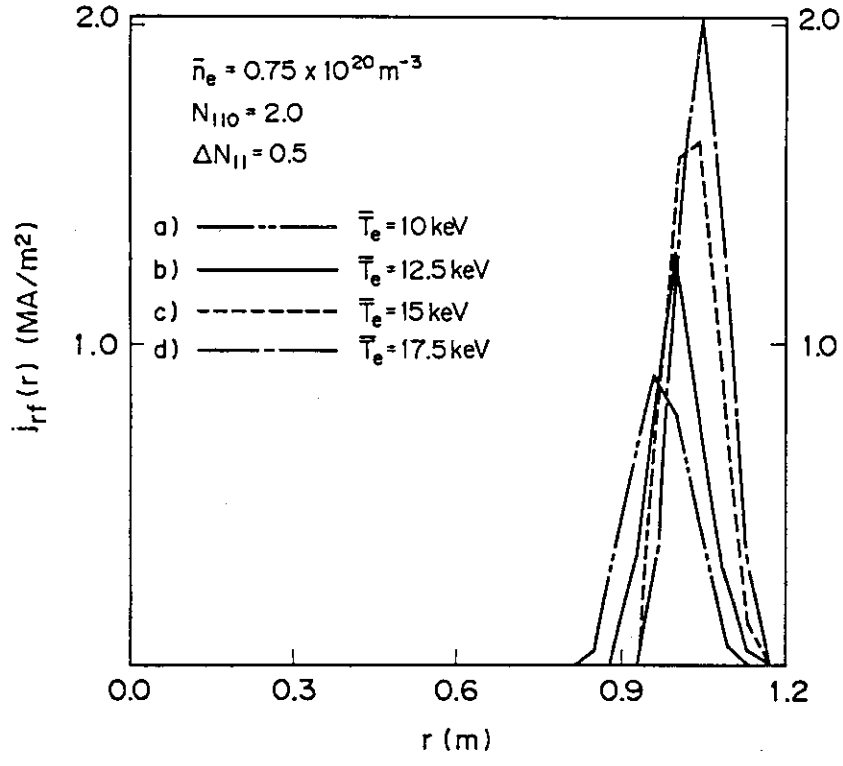

Fig. 8 Radial profile of the RF current for different average electron temperature; a) $\bar{T}_e$ = 10 keV, b) 12.5 keV, c) 15 keV and d) 17.5 keV, respectively. Average electron density is assumed to be constant ($\bar{n}_e = 0.75 \times 10^{20}$ m^{-3}).

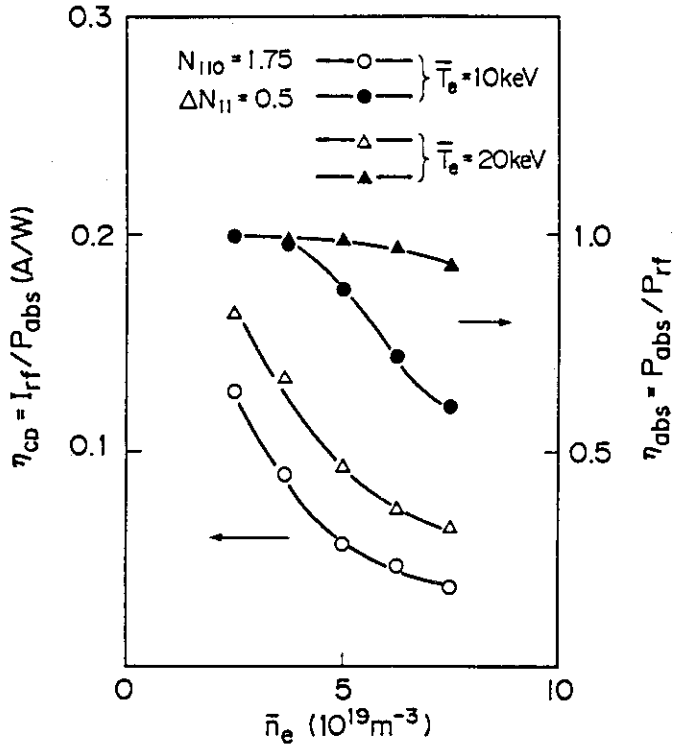

Fig. 9 Dependence of η_{cd} and η_{abs} on the average electron density $\bar{n}_e$ for $\bar{T}_e$ = 10 keV and 20 keV. Gaussian power spectrum with $N_{//0}$ = 1.75 and $\Delta N_{//}$ = 0.5 has been used.

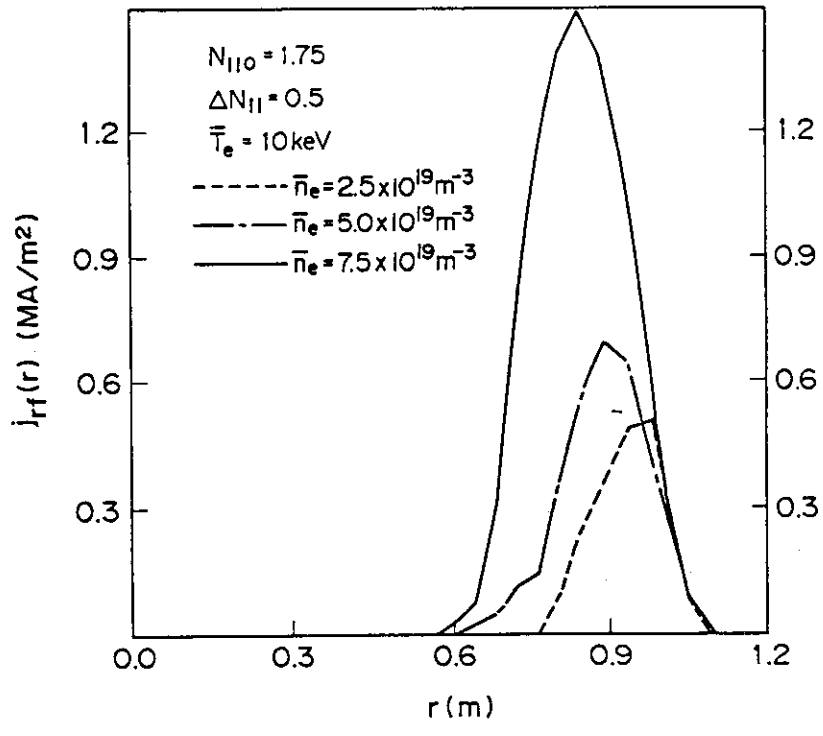

Fig. 10 Radial profiles of the RF current for different average density $\bar{n}_e$; a) $\bar{n}_e = 2.5\times10^{19}$ m^{-3}, b) $\bar{n}_e = 5.0\times10^{19}$ m^{-3} and c) $\bar{n}_e = 7.5\times10^{19}$ m^{-3}. Average electron temperature $\bar{T}_e$ is assumed to be constant ($\bar{T}_e$ = 10 keV).

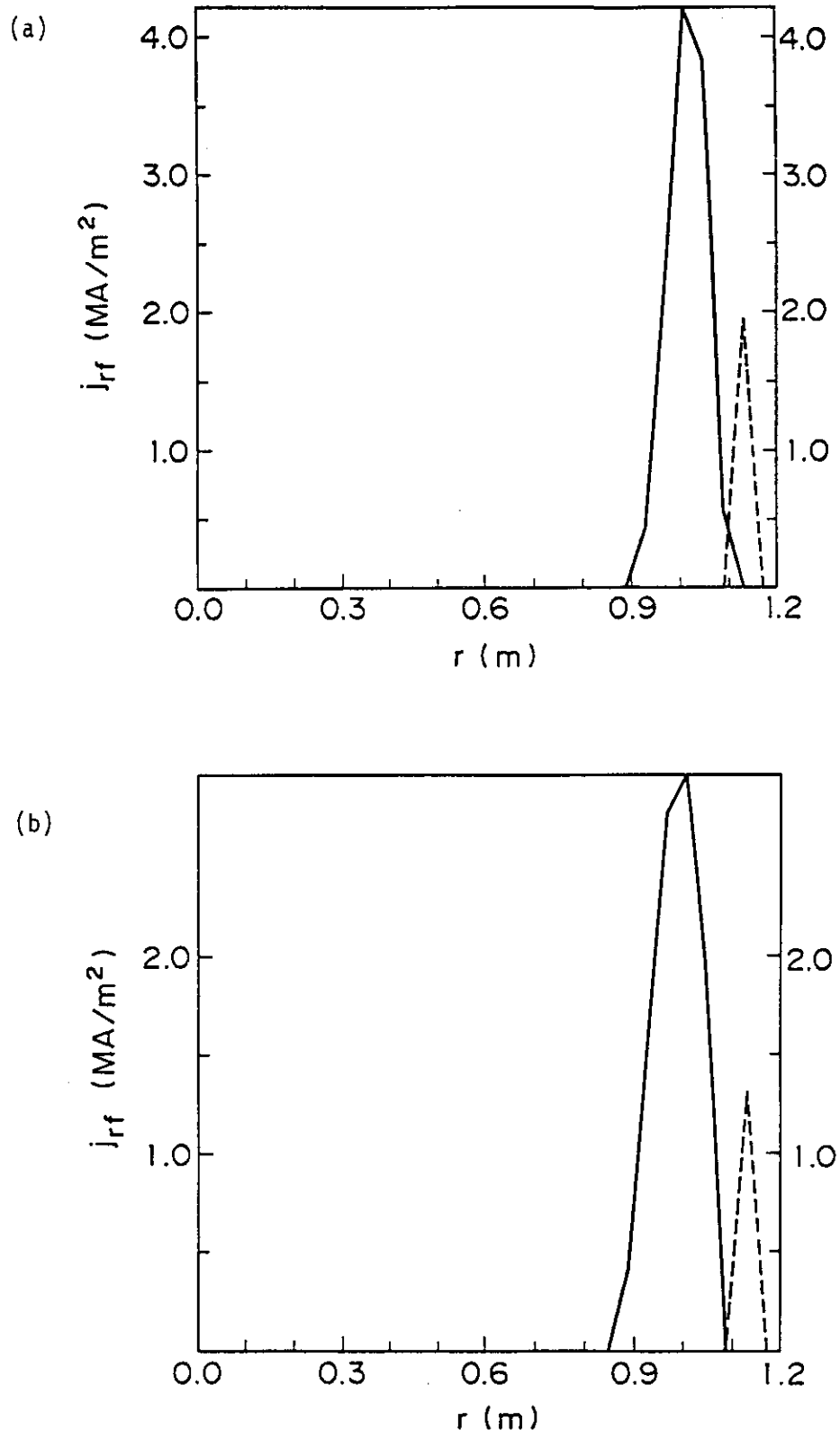

Fig. 11 RF current profile for horizontal launched case ($\theta_{inj}=0^{\circ}$). The launched spectra are calculated by Brambilla theory. Case (a) and (b) correspond to the case for $N_{/\!/0}$ = 2.0 and 1.8, respectively.

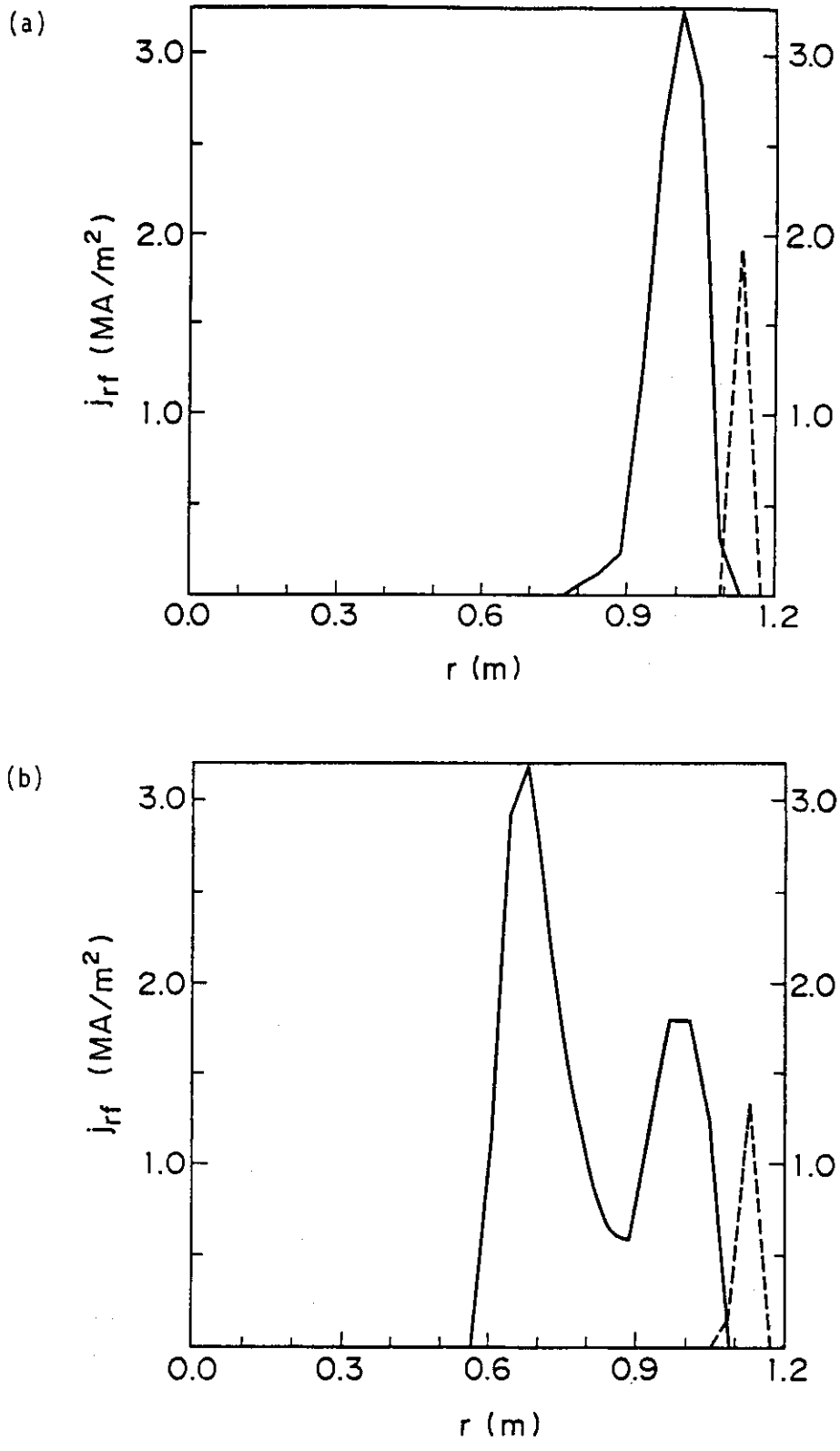

Fig. 12 RF current profile for top launched case (θ_{inj}=90^{o}). The launched spectra are calculated by Brambilla theory. Case (a) and (b) correspond to the case for $N_{//0}$ = 2.0 and 1.8, respectively.

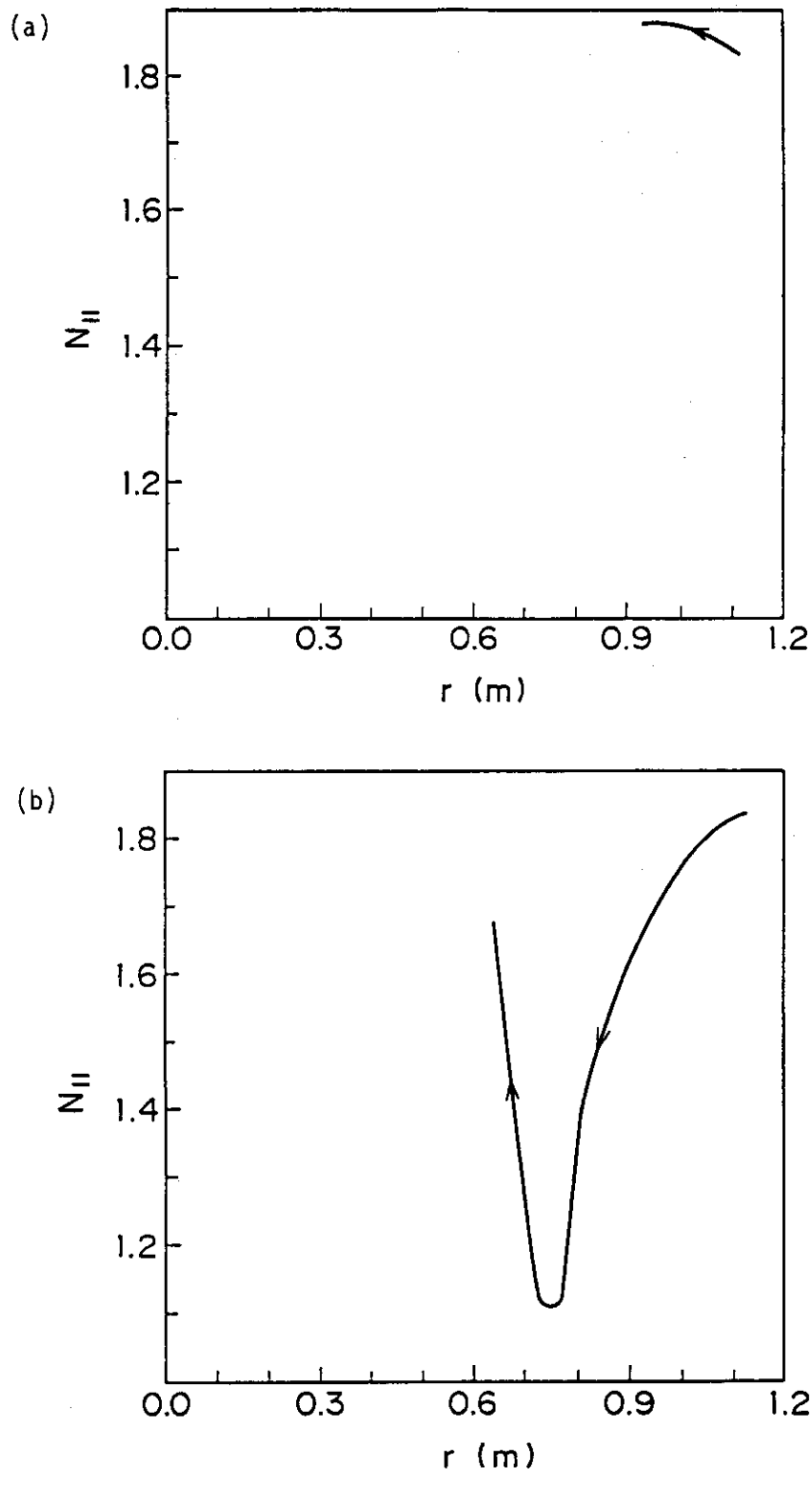

Fig. 13 Variation of $N_{/\!/}$ along the ray trajectory for (a) horizontal launched case ($\theta_{inj}=0^{o}$) and (b) top launched case ($\theta_{inj}=90^{o}$). The spectrum, which is initially launched with $N_{/\!/}$ = 1.834, has been effectively down-shifted in the interior of the plasma for the case (b).